Volumetric diffuse optical tomography of brain activity

Joseph P. Culver, Andrew M. Siegel, Jonathan J. Stott, and David A. Boas

Martinos Center for Biomedical Imaging, Massachusetts General Hospital, Harvard Medical School, Charlestown, Massachusetts 02129

We present three-dimensional diffuse optical tomography of the hemodynamic response to somatosensory stimulation in a rat. These images show the feasibility of volumetrically imaging the functional response to brain activity with diffuse light. A combination of positional optode calibration and contrast-to-noise ratio weighting was found to improve imaging performance. © 2003 Optical Society of America
   OCIS codes: 170.0170, 170.6510, 170.3880, 170.5270, 170.3660.

Novel hemodynamic contrasts and the portable, noninvasive character of diffuse optical imaging motivate its recent application to functional brain imaging of a variety of mental activations, including motor,[1] visual,[2] auditory,[3] and language[4] activations. However, because of the remission geometry usually required,[5] there has been limited three-dimensional diffuse optical tomography (DOT) of the brain.[6] The sensitivity of diffuse-light measurements drops off quickly with increased depth. In addition, the fast data acquisition rates required for functional activation studies ($\tau_{\mathrm{frame}} < 1$ s) limit the number of optode measurement pairs. Finally, head structures require conformable probe assemblies, and information about the positions and directions of the optodes becomes critical. We have addressed these challenges by using a fast imaging system and creating algorithms to manage the bias of images toward the optode locations. A positional calibration (PC) algorithm was used to determine the true optode positions by minimization of the correlated errors in light intensity induced by displacement of individual optodes from the modeled positions.[7] In addition, spatially variant contrast-to-noise ratio (CNR) weighting was used to flatten the sensitivity profile of the inversion. These imaging methods were first evaluated on simulated data and then used to image the functional activation of the somatosensory cortex in a rat during forepaw stimulation.

The diffuse optical measurements employed a frequency-encoded cw imaging system with nine dual-wavelength sources (laser diodes at 690 and 830 nm) and 16 detectors (avalanche photodiodes).[8] The light sources and detectors were coupled through 100-μm optical fibers and held in contact with the scalp of an anesthetized rat by use of a conformable rubber pad (Fig. 1). The optode array covered a flat region of the rat's head extending 7.5 mm on either side of the midline and from 4 mm anterior to 11 mm posterior of the bregma. Electric stimulation of the forepaw was applied by constant current pulses (200 μs, 1.0 mA, 3 Hz repetition) with 6-s duration and a 54-s interstimulus interval. Measurements of 32 stimulus blocks were averaged, and activation was defined with a shifted 6-s bin to capture the peak change in differential intensity.

To find the optode positions, we exploited the correlated errors in the measurements caused by the displacements of individual optodes. If, for example, a center source were displaced to the left of the expected grid position, then the light intensity would slightly increase in the detectors to the left and decrease in the detectors to the right. We fit for the positional calibrations within the xy plane by minimizing the amplitude error between the baseline light levels and model predictions (see below) with a Levenberg–Marquardt minimization algorithm. The source and detector optode coupling coefficients and the effective attenuation coefficient (k) were also deduced from the fitting procedure.[9]

Photon migration was modeled with the semi-infinite media extrapolated zero boundary condition solution.[10] The fluence rate, Φ_i, is determined by a point-source amplitude, S_0; positions of a source, $\mathbf{r}_{s(i)}$ and a detector $\mathbf{r}_{d(i)}$; and the tissue's optical properties, represented by μ_a and μ_s', the tissue absorption and reduced scattering coefficients, respectively.

Differential images were reconstructed with the Rytov approximation,[11] $\Phi = \Phi_o \exp(\Phi_{\mathrm{scat}})$, where Φ_o is the background fluence and Φ_{scat} is the differential fluence due to spatiotemporal variations in absorption, $\delta\mu_a$. In discrete notation, $\mathbf{y} = \mathbf{Ax}$, the Rytov formulation has the following definitions:

$$y_i = \ln[\Phi(\mathbf{r}_{s(i)}, \mathbf{r}_{d(i)})/\Phi_o(\mathbf{r}_{s(i)}, \mathbf{r}_{d(i)})],$$

$$\begin{aligned}A_{i,j} = (-\nu h^3/D_o) \\ \times G(\mathbf{r}_{s(i)}, \mathbf{r}_j)G(\mathbf{r}_j, \mathbf{r}_{d(i)})/G(\mathbf{r}_{s(i)}, \mathbf{r}_{d(i)}),\end{aligned}$$

and $x_j = \delta\mu_{aj}$. The Green's function, G, satisfies the extrapolated zero boundary condition. The following baseline optical properties were assumed[8,12]: $\mu_{s,\lambda=690\,\mathrm{nm}}' = 18$ cm^{-1}, $\mu_{s,\lambda=830\,\mathrm{nm}}' = 16$ cm^{-1}, $\mu_{a,\lambda=690\,\mathrm{nm}} = 0.21$ cm^{-1}, and $\mu_{a,\lambda=830\,\mathrm{nm}} = 0.22$ cm^{-1}. The absorption values were calculated assuming a total hemoglobin concentration of [HbT] = 100 μM
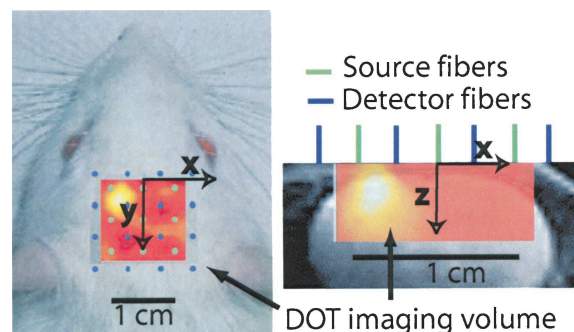

Fig. 1. DOT of rat brain function, fiber array positions, and imaging domains. Left, horizontal (xy); right, coronal (xz).

and 70% oxygen saturation.[8,12] An image reconstruction solution, $\mathbf{x} = \mathbf{A}_\alpha^\# \mathbf{y}_{\mathrm{meas}}$, was obtained with a Moore–Penrose generalized inverse with $\mathbf{A}_\alpha^\# = L^{-1}\tilde{\mathbf{A}}^T(\tilde{\mathbf{A}}^T\tilde{\mathbf{A}} + \alpha I)^{-1}$, where $\tilde{\mathbf{A}} = \mathbf{A}L^{-1}$ and L was constructed with spatially variant regularization.[12] Voxels, 0.5 mm on an edge and spanning an 18 mm × 6 mm × 18 mm volume ($\sim 1.5 \times 10^4$ voxels), were used with 100 measurements. For analysis we extracted a smaller volume that was well supported by multiple source detector pairs that extended from 2 mm anterior to 10 mm posterior of the bregma, ±6 mm laterally of the midline, and over depths of 0–4.5 mm. Computation of $\mathbf{A}_\alpha^\#$ for each method took 14 s on a 1.8-GHz AMD Athlon MP machine. With direct inversion, $\mathbf{A}_\alpha^\#$ was computed once and then applied to the entire measurement time series.

To evaluate the PC algorithm, we simulated data with optodes displaced from regular grid positions in the xy plane with a mean random displacement error of 0.7 mm. Random coupling coefficients for each source, $C_{s(i)}$, and detector, $C_{d(i)}$, optode were multiplied by each optode pair intensity. Additionally, we added 2% random noise (e_i) to each pair [$I_i^{\mathrm{sim}} = C_{s(i)}C_{D(i)}I_i^{\mathrm{DPDW}}(1 + e_i)$]. Whereas the random optode coupling coefficients were, by definition, correlated to individual optodes, the pairwise applied random noise was uncorrelated to specific optodes. Values of the random displacement error and variance in optode coupling were obtained from baseline *in vivo* rat measurements. Application of the PC routine reduced the mean displacement error to 0.07, an $\sim 10\times$ reduction.

The reconstruction procedures were evaluated. Three simulated test point objects were used with differential signals equal in magnitude to those found in the experimental data (maximum) ($\Delta I/I = 1\%$). Gaussian random noise (0.01%) was added to the data based on noise levels in the block-averaged experimental data. In addition, ten frames of baseline noise-only data were inverted, from which an image of the standard deviation at each pixel was constructed. Spatially variant CNR (SV-CNR) weighting was achieved by division of an activation image by a standard deviation image. Spatially flat CNR (F-CNR) weighting was obtained by division of an activation image by the mean value of an entire standard deviation image. Four image reconstruction schemes were evaluated. First, the data were inverted with a sensitivity matrix ($\mathbf{A}$) constructed with the PC optode positions and SV-CNR weighting [Fig. 2(a)]. The activation is clearly resolved in three dimensions. Images were also reconstructed with the three alternate permutations of with and without PC and SV-CNR or F-CNR weighting. For all images the regularization constant was set at 0.5×10^{-3} times the first singular value. With no PC and with F-CNR weighting, depth localization was poor [Fig. 2(b)]. To assess the image quality, we calculated the center of activation with a weighted positional average of the contrast, and we calculated the activation volume, defined as the volume greater than 50% peak contrast (Table 1).

Experimental images of the hemodynamic response to forepaw stimulation are shown in Fig. 3. *In vivo* baseline light intensities were used with the PC algo-

rithm to find the corrected optode positions [Fig. 3(c)]. Reconstructions of $\delta\mu_{a,\lambda=690\,\mathrm{nm}}$ and $\delta\mu_{a,\lambda=830\,\mathrm{nm}}$ were performed with the PC algorithm and SV-CNR weighting. Images of the left [Fig. 3(a)] and the right [Fig. 3(b)] forepaw activations (CNR of $\delta\mu_{a,\lambda=830\,\mathrm{nm}}$) show foci at depths of 1.6 and 2.3 mm, respectively. The lateral displacement between the left and right
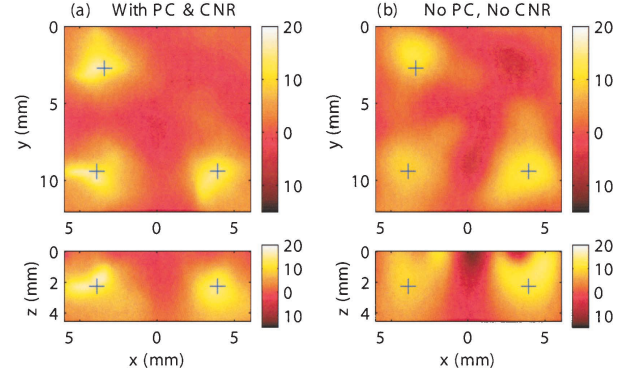

Fig. 2. Image reconstruction methods were evaluated with simulations. (a) CNR in $\delta\mu_a$ with PC and SV-CNR weighting, xy slice at $z = 2.25$ mm and xz slice at $y = 9.5$ mm. (b) CNR in $\delta\mu_a$ without PC and without SV-CNR (e.g., constant) weighting. Color bars state CNR.

Table 1. Comparison of Reconstruction Methods

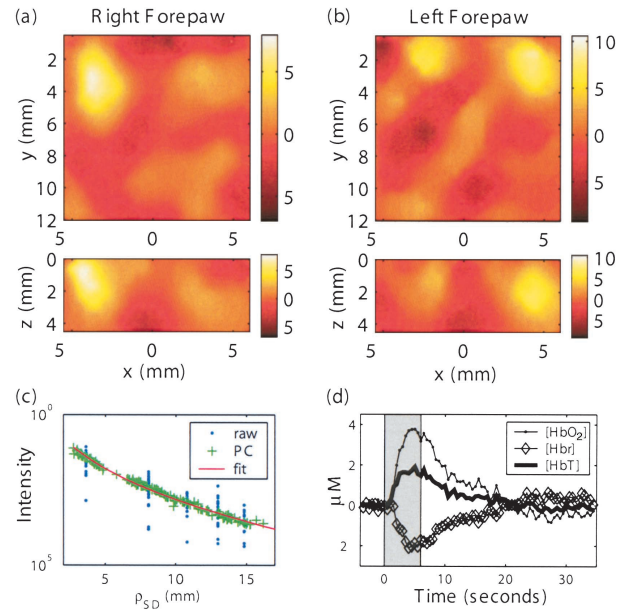| Method	Δz (mm)	$\Delta|\mathbf{r}|$ (mm)	Volume (mm^3)
PC and CNR	0.1 ± 0.1	0.5 ± 0.2	11.8 ± 4
PC and no CNR	-0.6 ± 0.1	0.7 ± 0.1	27.8 ± 14
No PC and CNR	0.3 ± 0.2	0.5 ± 0.2	12.4 ± 8
No PC and no CNR	-1.3 ± 0.5	2.4 ± 2.0	32 ± 23

Fig. 3. Experimental DOT images of CNR in $\delta\mu_{a,\lambda=830\,\mathrm{nm}}$ during rat brain activation. (a) Right forepaw, xy slice at $z = 1.75$ mm, xz slice at $y = 2$ mm. (b) Left forepaw, xy slice at $z = 2.25$ mm, xz slice at $y = 2$ mm. (c) Calibration of optode positions by use of baseline intensities. (d) Activation time traces of [HbR], [HbO$_2$], and [HbT].
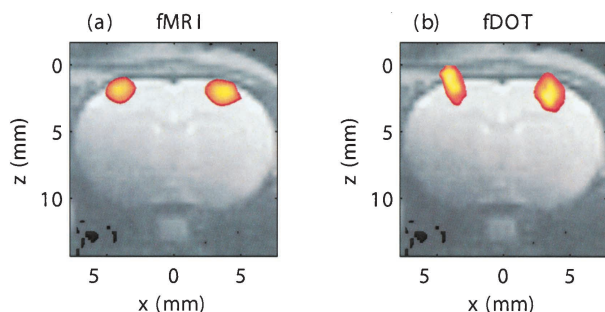
Fig. 4. (a) fMRI activation images (CNR of cerebral blood volume) are overlaid on MRI anatomy. (b) For illustrative comparison functional DOT (fDOT) (CNR of $\delta\mu_{a,\lambda=830\,\mathrm{nm}}$) activations from Fig. 3 (combined right and left forepaw) are overlaid on the same MRI anatomy.

activations is 6.8 mm and the half-maximum volumes are 14 and 11 mm^3, respectively. Time courses of the hemoglobin concentrations in the activation volume were also computed [Fig. 3(d)]. Absorption traces, $\delta\mu_a(t)$, in the activation volume (2 mm $\times$ 2 mm $\times$ 2 mm volumes centered on the peak value) were extracted from image series at each wavelength. Peak values at $T = 5.5$ s were $\delta\mu_{a,\lambda=690\,\mathrm{nm}} = -0.007$ cm^{-1} and $\delta\mu_{a,\lambda=830\,\mathrm{nm}} = 0.006$ cm^{-1}. Hemoglobin concentrations, deoxy-[Hbr], oxy-[HbO], and total-[HbT], were obtained with spectral decomposition.[8]

From the simulations it is clear that SV-CNR weighting improves both the depth positioning and the point-spread function (volume). When activation images are divided by a standard deviation image, the increased sensitivity near the optodes is normalized by the increase in image noise near the optodes. This weighting reduces the effect of image bias toward the surface and improves depth localization. We also find improved image metrics when using the corrected optode positions. This is more significant for the images with F-CNR weighting, although improvement is also apparent with SV-CNR weighting. Incorrect optode positions introduce model errors and disrupt the synthesis of the individual measurements into an image. We found displacement errors of ~0.68 mm for our experimental setup, which is ~20% of the shortest interoptode distance ($\rho_{\mathrm{sd}} = 3.6$ mm). On humans this would correspond to a 6-mm displacement error for a 3-cm source detector separation, which is a reasonable positional error. Concurrent magnetic resonance imaging (MRI) scans can measure optode locations, but positional mismatches of 1–4 mm between magnetic resonance markers and optode tips can easily occur. As data averaging improves, imaging artifacts caused by displaced optodes become more limiting, and optode PC provides a simple solution to these issues.[7]

We compared our optical images with functional MRI (fMRI) images of the same rat forepaw stimulation protocol.[13] Contrast-agent-based fMRI cerebral blood volume images locate the activation at a depth of 2.15 $\pm$ 0.2 mm, with a separation between left and right forepaw activations of 7.5 $\pm$ 0.1 mm and an activation FWHM of 1.4 $\pm$ 0.1 mm [Fig. 4(a)]. Our results are in good agreement with the lateral separation between the activation volumes and the

depth locations [Fig. 4(b)]. We found the DOT activation volume to have an ~70% larger FWHM (FWHM = $\sqrt[3]{13}$ = 2.4 mm), which is consistent with the point-spread functions found in the simulations. The slight positional shifts relative to fMRI may be caused by either residual method and modeling errors, interanimal variability, or differences in the vascular weightings of the two imaging modalities. All three issues are significant and warrant more extensive studies with concurrent DOT and fMRI.

Previously, we reported DOT images of brain function constrained to a two-dimensional layer.[8] In addition, we evaluated the correlation of the DOT temporal response ($n = 4$ rats) with a previous fMRI study. Here we have extended image reconstruction analysis to three-dimensional volumetric imaging. Functional images were constructed of a relatively small ($\Delta I/I = 1\%$), though well-characterized and focal, hemodynamic perturbation. The images demonstrate the feasibility of volumetrically imaging the hemodynamic responses to brain activity. We anticipate that the reported DOT methods will be useful in addressing functional imaging questions in a wide range of applications including stroke, epilepsy, and brain development.

References

1. M. A. Franceschini, V. Toronov, M. E. Filiaci, E. Gratton, and S. Fantini, Opt. Express **6,** 49 (2000), http://www.opticsexpress.org.
2. W. Colier, V. Quaresima, R. Wenzel, M. C. van der Sluijs, B. Oeseburg, M. Ferrari, and A. Villringer, Vision Res. **41,** 97 (2001).
3. P. Zaramella, F. Freato, A. Amigoni, S. Salvadori, P. Marangoni, A. Suppjei, B. Schiavo, and L. Chiandetti, Pediatr. Res. **49,** 213 (2001).
4. K. L. Sakai, R. Hashimoto, and F. Homae, Neurosci. Res. **39,** 1 (2001).
5. J. P. Culver, V. Ntziachristos, M. J. Holboke, and A. G. Yodh, Opt. Lett. **26,** 701 (2001).
6. A. Y. Bluestone, G. Abdoulaev, C. H. Schmitz, R. L. Barbour, and A. H. Hielscher, Opt. Express **9,** 272 (2001), http://www.opticsexpress.org.
7. J. J. Stott, J. P. Culver, S. R. Arridge, and D. A. Boas, Appl. Opt. **42,** 3154 (2003).
8. A. M. Siegel, J. P. Culver, J. B. Mandeville, and D. A. Boas, Phys. Med. Biol. **48,** 1391 (2003).
9. D. A. Boas, T. Gaudette, and S. R. Arridge, Opt. Express **8,** 263 (2001), http://www.opticsexpress.org.
10. C. Cheung, J. P. Culver, A. G. Yodh, K. Takahashi, and J. H. Greenberg, Phys. Med. Biol. **46,** 2053 (2001).
11. M. A. Oleary, D. A. Boas, B. Chance, and A. G. Yodh, Opt. Lett. **20,** 426 (1995).
12. J. P. Culver, T. Durduran, D. Furuya, C. Cheung, J. H. Greenberg, and A. G. Yodh, J. Cereb. Blood Flow Metab. **23,** 911 (2003).
13. J. B. Mandeville and J. J. Marota, Magn. Reson. Med. **42,** 591 (1999).